

DTIC FILE COPY

2

Naval Ocean Research and Development Activity

August 1989

Report 223



**Evidence for Self-Refraction in a Convergence Zone:
NPE Model Results**

AD-A218 546

DTIC
ELECTE
FEB 28 1990
S E D
CD

B. Edward McDonald
Ocean Sensing and Prediction Division
Ocean Science Directorate

Daniel R. Plante
Berkeley Research Associates
Springfield, VA 22150

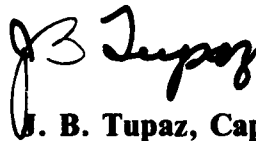
90 02 26 091

Foreword

When a shock wave propagates in the deep-ocean sound channel, overpressure and/or impulsive translational velocity may be of concern to safe standoff at convergence zone ranges (30-50 km). The wave's nonlinearity may produce long-range propagation effects not described by linear acoustic models. NORDA's nonlinear progressive wave equation (NPE) model is being tested for use by Sandia National Laboratory in predicting the evolution of nonlinear waves over long propagation paths. Contemporary hydrocodes would be of questionable utility in this problem because of their high operation count and low sensitivity to small but cumulative environmental effects. This report presents numerical results from the NPE model that illustrate nonlinear effects for an ideal and a realistic ocean sound speed profile. One of these effects has been identified as self-refraction, i.e., the wave's alteration of its own ray paths. Self-refraction is to be expected on theoretical grounds, but has not previously been demonstrated in long-range propagation results.



W. B. Moseley
Technical Director



J. B. Tupaz, Captain, USN
Commanding Officer

Executive Summary

The nonlinear progressive wave equation (NPE) model was developed by the Naval Ocean Research and Development Activity during 1982-1987 to study nonlinear effects in long-range oceanic propagation of finite amplitude acoustic waves, including weak shocks. The NPE model has been applied to propagation of a generic shock wave (initial condition provided by Sandia Division 1533) in a few illustrative environments. The following consequences of nonlinearity are seen by comparing linear and nonlinear NPE results: (1) a decrease in shock strength versus range (a well-known result of entropy increase at the shock front); (2) an increase in the convergence zone range; and (3) a vertical meandering of the energy path about the corresponding linear ray path. Items (2) and (3) are manifestations of self-refraction.

| | |
|--------------------|-------------------------------------|
| Accession For | |
| NTIS GRA&I | <input checked="" type="checkbox"/> |
| DTIC TAB | <input checked="" type="checkbox"/> |
| Unannounced | <input type="checkbox"/> |
| Justification | |
| By _____ | |
| Distribution/ | |
| Availability Codes | |
| Dist | Avail and/or Special |
| A-1 | |



Acknowledgment

This work was supported by Sandia National Laboratory via Sandia Document 63-5837, utilizing technology developed with the support of the Defense Nuclear Agency and the Office of Naval Research.

Contents

| | |
|---|---|
| 1.0 Introduction | 1 |
| 2.0 Shock Propagation Calculations | 1 |
| 2.1 Case 1—Control | 2 |
| 2.2 Case 2—Optimal Convergence | 2 |
| 2.3 Case 3—A Realistic Sound Channel | 5 |
| 3.0 Summary | 5 |
| 4.0 References | 8 |

Evidence for Self-Refraction in a Convergence Zone: NPE Model Results

1.0 Introduction

The present approach¹ to modeling long-range nonlinear wave propagation was developed as a means of including finite amplitude effects (wave steepening and shock physics) in a multidimensional model which recovers known acoustic limits in the far field. The nonlinear progressive wave equation (NPE) model has been derived from hydrodynamic equations to describe outgoing waves propagating near Mach 1. The model can also be derived from a first integral of nonlinear wave equations used previously.^{2,3} The NPE has been shown⁴ to be the nonlinear time domain counterpart of the frequency domain parabolic wave equation (PE). For an azimuthally symmetric ocean, the three-dimensional NPE reduces to the initial value problem

$$\frac{DR}{Dt} = \frac{\partial}{\partial r} \left(c_1 R + c_0 \frac{\beta}{2} R^2 \right) - \frac{c_0}{2} \frac{R}{r} - \frac{c_0}{2} \int_{r_f}^r \frac{\partial^2 R}{\partial z^2} dr, \quad (1)$$

where r is horizontal range from the source, z is depth, and

$$R \equiv \rho' / \rho_0 \quad (2)$$

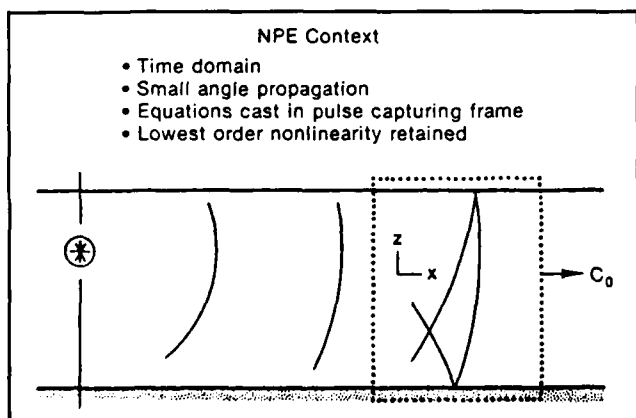


Figure 1. The NPE model is executed in a grid (dotted lines) moving at constant average sound speed c_0 with respect to the medium.

is the acoustic density fluctuation about the local environmental value. The time derivative

$$\frac{D}{Dt} \equiv \frac{\partial}{\partial t} + c_0 \frac{\partial}{\partial r} \quad (3)$$

is evaluated in a wave-following frame of reference (Fig. 1) moving at the constant average sound speed c_0 ; c_0 and $c_1(r, z)$ are user-supplied values such that the range-dependent environmental linear sound speed is $c(r, z) = c_0 + c_1(r, z)$. The coefficient of nonlinearity β is taken to be 3.5 for the ocean. The lower limit of integration r_f is taken in the quiescent medium just ahead of the wave. The moving grid uses a reduced range coordinate, $x \equiv r - c_0 t$.

2.0 Shock Propagation Calculations

Figure 1 illustrates the moving NPE grid used in the calculations. For the cases presented here, the grid consists of 351 by 376 points with horizontal and vertical mesh resolution of 3 m and 16 m, respectively. The grid window is thus 1.05 km wide and 6 km deep. Calculations were made on a Cray 1S at Sandia-Livermore, requiring an average of 45 CPU minutes per case for propagation out past 60 km. Propagation to 60-km range is accomplished in approximately 1400 to 1600 timesteps. A spherical shock wave descriptive of a low- to medium-yield device (100- to 200-kt range) is taken to be the initial condition for calculations in this report. More accurate specification of yield is not necessary for illustrative purposes, since overpressure at fixed range is expected to scale roughly with the cube root of the yield. In deference to the paraxial approximation inherent in the NPE, the initial disturbance is cut off outside an annulus of propagation angles within $\pm 63^\circ$ of horizontal. Numerical benchmarks against linear analytic solutions confirm that high-angle wave components surviving this truncation quickly fall behind the moving grid (and thus do not contaminate results) because of their decreased horizontal group velocity. The initial radial profile of the shock over-density $R = \rho' / \rho_0$ is shown in Figure 2. The radius of the shock is 280 m, and the peak over-density 0.044 behind the shock corresponds to an overpressure of

1.13 kbar (one atmosphere is 1.013 bar). For the pressure range applicable to this source, overpressures p' and particle velocities v may be obtained from overdensities via (almost) linear algebraic formulae. An overdensity of 10^{-3} gives an overpressure of 22.5 bar and a particle speed of 1.5 m/sec, or about 5 ft/sec. For water we assume nominal values for sound speed $c_0 = 1500$ m/sec and bulk modulus $\rho_0 c_0^2 = 22.5$ kbar. At higher pressures, the Tait equation of state for p' and a one-dimensional similarity solution for v are used:

$$\frac{p'}{\rho_0 c_0^2} = \frac{1}{n} ((1 + R)^n - 1)$$

$$v = \int \frac{c \, d\rho}{\rho}$$

$$= \frac{2c_0}{n-1} \left((1 + R)^{\frac{n-1}{2}} - 1 \right),$$

$$n = 7.15 \quad (4)$$

2.1 Case 1—Control

A control calculation was performed for isovelocity water ($c_1 = 0$) with the source at 1000-m depth. The resulting peak overdensity R_{max} behind the shock is shown versus range in Figure 3. For $r > 1$ km, the result closely approximates the empirical $r^{-1.13}$ power law observed for overpressures in experiments using high explosives. The distinction between overpressure

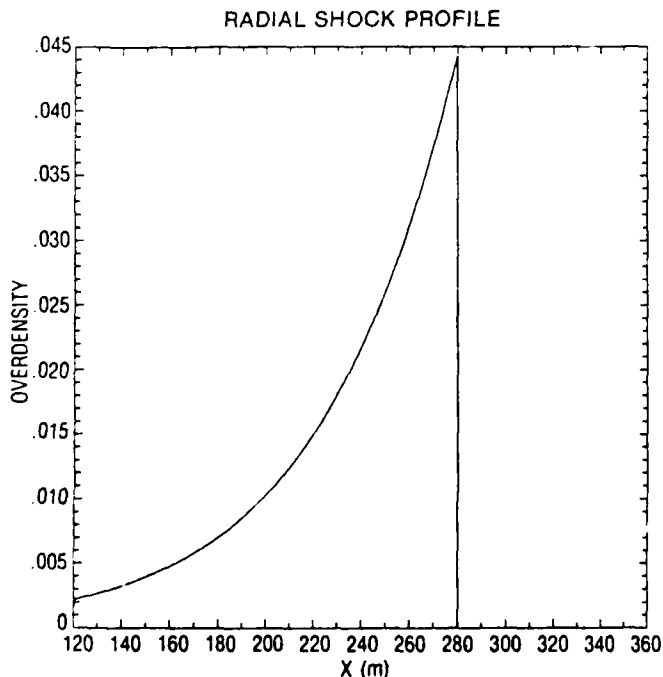


Figure 2. Radial variation of water overdensity in a spherical shock descriptive of a 100- to 200-kt device. The peak overpressure is 1.13 kbar, or 281 dB re $1\mu\text{Pa}$.

(normalized to bulk modulus) and overdensity is negligible for this range of values. This test shows that the model does not suffer from excessive numerical dissipation, although local filtering in the form of flux correction is used to prevent parasitic oscillations near shock fronts.

2.2 Case 2—Optimal Convergence

The "ideal sound channel" according to linear ray theory is of the form $c(z) = c_{min} \cosh(\pi z/r_{cz})$. Rays from a point source at $(r, z) = (0, 0)$ meet perfectly at a convergence point $(r_{cz}, 0)$. Although nature does not produce smooth, ideal sound channels, this case helps answer the question, What are the limiting effects at convergence of a given source at a given depth? Comparison of ideal and realistic sound channels can also give an indication of the sensitivity of results to environmental changes. Figure 4 gives an ideal sound channel whose axis is at depth 1000 m for $c_{min} = 1480$ m/sec and $r_{cz} = 50$ km. Three NPE calculations for on-axis sources were performed for sources scaled to peak overdensities 0^+ , 0.044, and 0.2, corresponding to peak pressures 0^+ , 1.13, and 8.44 kbar at 280-m radius. These illustrate the effects of nonlinearity on the convergence zone. The 0^+ scaling refers to a linear calculation done by deleting the nonlinear term from the NPE. Linear results may be normalized arbitrarily for comparison with nonlinear results. These three sources are denoted below as Linear, 1 kbar and 8 kbar.

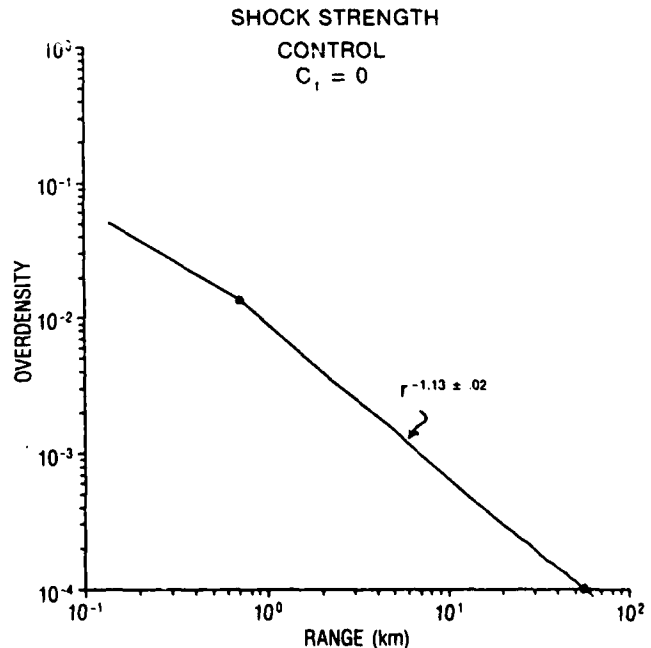


Figure 3. NPE model result for peak overdensity versus range resulting from the shock wave of Figure 2 in isovelocity water. This result agrees closely with empirical power law behavior observed with high explosive charges.

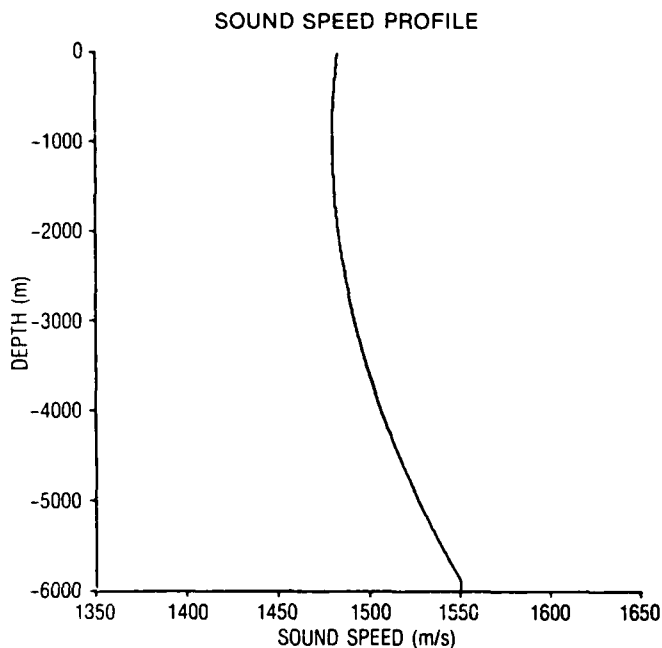


Figure 4. "Perfect" sound channel for a source at the 1000-m depth. Convergence zone is at 50-km range.

Figure 5a gives peak overdensities and particle speeds v_{max} versus range. Convergence zone focusing near 50-km range is evident for all three source levels. Note the increased transmission loss in the nonlinear cases relative to the linear case (the separation between the three curves diminishes with range). This increase is a physical result of wave energy being lost to dissipative heating at the shock front. In all three cases, the full width at half-maximum of the focal region is approximately 10 km. For the 1-kbar source, an impulsive particle speed of 2 ft/sec behind the shock occurs at range \sim 53 km. The corresponding overpressure is 9 bars. Close inspection of Figure 5a reveals an increase of focal range with increased source strength, and is more evident in the semilog plot of Figure 5b than in the log-log plot of Figure 5a. This manifestation of a nonlinear effect is known as self-refraction. Increasing the amplitude from the Linear to the 1-kbar source increases the focal range about 5 km, or 10%. The reason the focal range increases with amplitude is that until the shock is quite weak, the nonlinear contribution to the sound speed overshadows the environmental variation within the sound channel. This results in an effective delay in environmental focusing effects. An additional increase to the 8-kbar source broadens the focal region, but interestingly does not appear to increase the focal range significantly. This point deserves further investigation.

Figure 6 shows overpressure contours at times corresponding to propagation ranges of 6.54, 37.74, 58.25, and 65.28 km for the 8-kbar source in the idealized sound channel of Figure 4. The 8-kbar

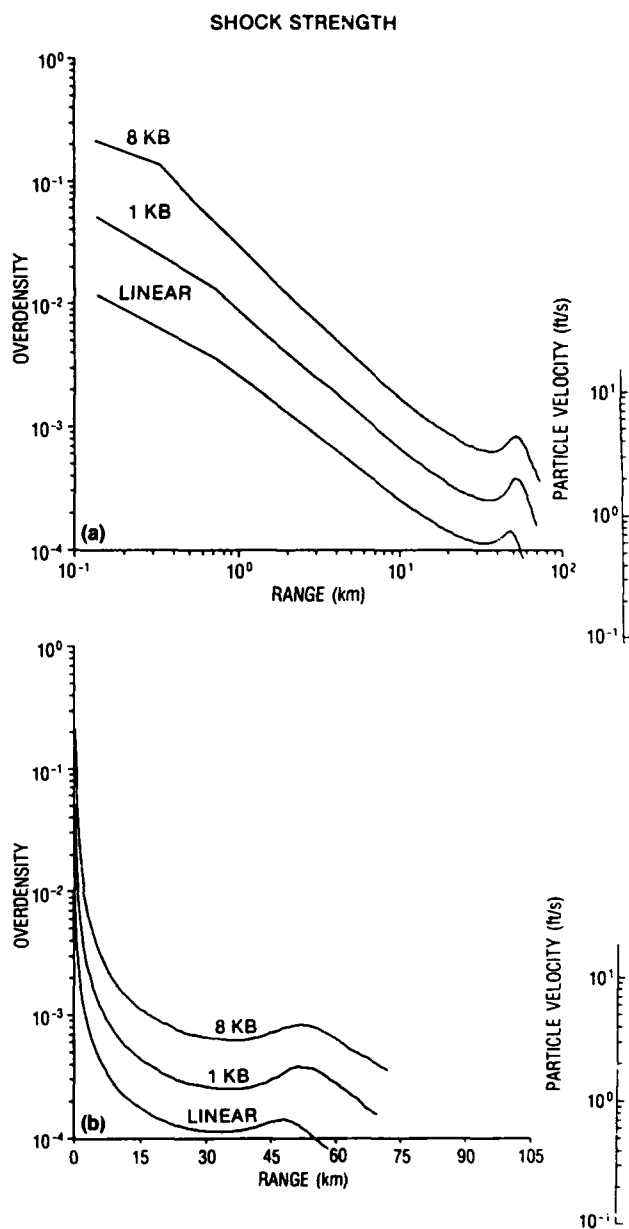


Figure 5. (a) Peak overdensity versus range for initial source pressures 1.13 and 8.44 kbar. A linear calculation is added (normalized arbitrarily) to show trends in nonlinear attenuation and focal range. (b) Same curves plotted semilog to show increase in focal range and width of focal region with increased source level.

calculation illustrates the peak pressure point's meander around the direct ray path. Note the rise above the sound channel axis past the 50-km convergence. This is another manifestation of self-refraction; i.e., the ray path is affected by the amplitude of the wave. Similar calculations (contour plots not given here) for Linear and 1-kbar sources show a monotonic increase in meander with increasing source strength. This is

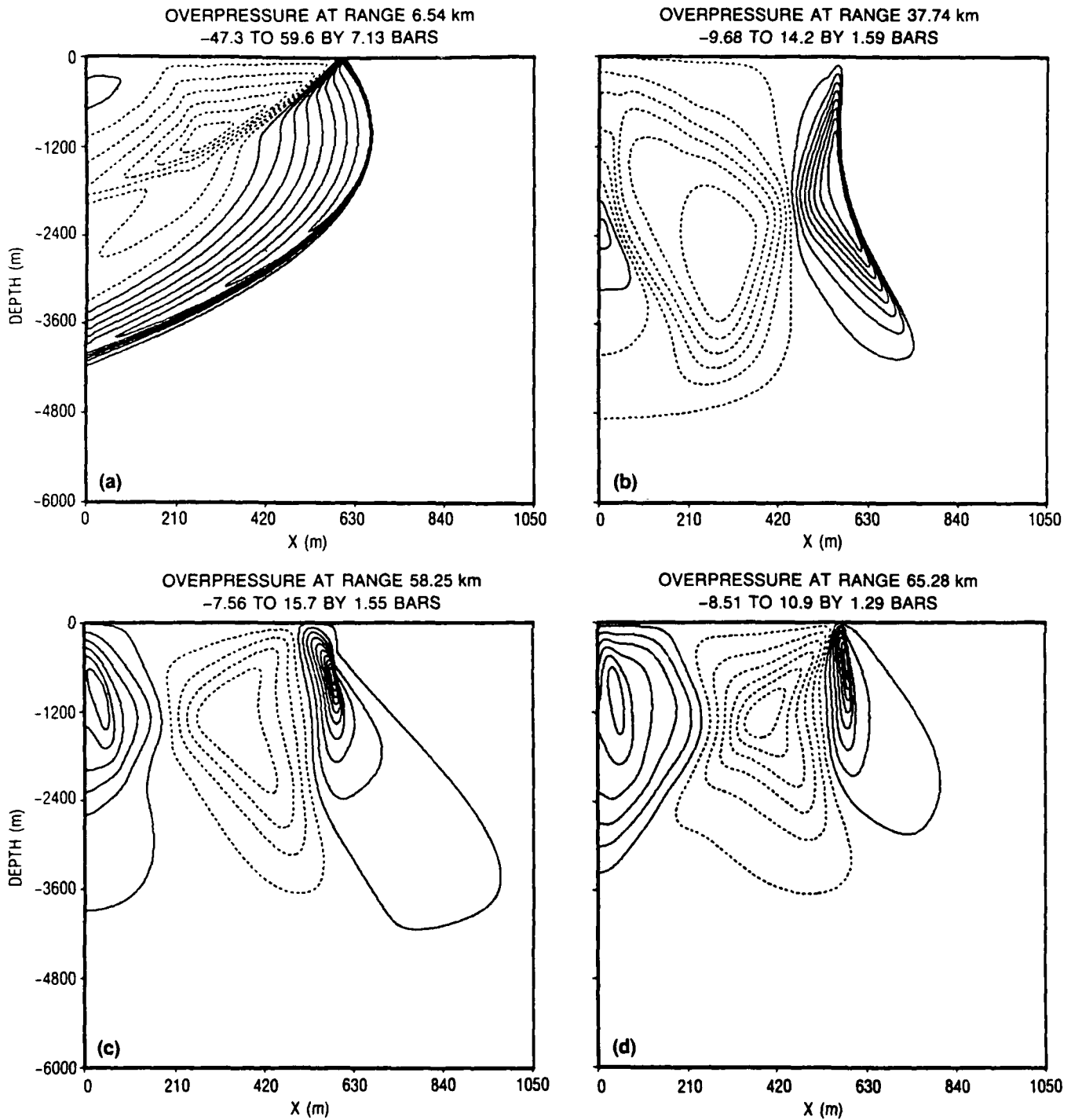


Figure 6. Contour plots (snapshots) of overpressure during propagation through a convergence zone of the "perfect" sound channel of Figure 4. The source depth is 1000 m, and the initial pressure level 8.44 kbar.

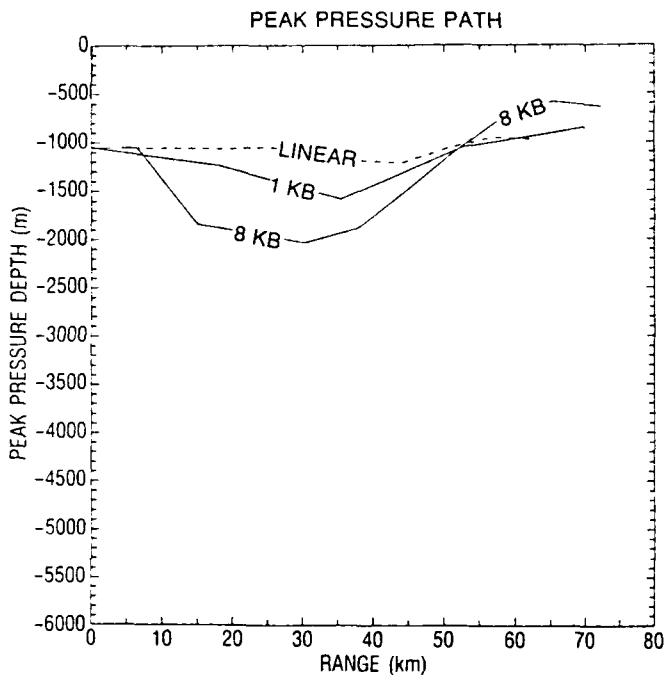


Figure 7. Meandering of the peak pressure point about the axis of a "perfect" sound channel from Figure 6 and from calculations at two other source levels. Linear ray theory in the absence of a free surface predicts a straight line along the channel axis.

shown in Figure 7 where the depth of the visible centroid of the maximum pressure contour is plotted against range for Linear, 1-kbar, and 8-kbar sources. The linear path reasonably follows the channel axis in agreement with ray-trace predictions, until approximately 30 km, when the surface reflection begins to interfere. The three curves for Linear, 1-kbar, and 8-kbar sources effectively meet just past the 50-km linear convergence zone. Past this point, the peak pressure path moves closer to the surface with increasing source strength. Figures 5, 6 and 7 contain possibly the first demonstration of self-refraction in a long-distance propagation calculation. It has, however, been seen in a steady-state, boundary-forced calculation.¹ Experimental observation of this effect apparently has not been attempted (A. V. Farnsworth, Sandia Laboratories, private communication, 1988).

2.3 Case 3—A Realistic Sound Channel

Figure 8 shows a real ocean sound speed profile taken in winter near Bermuda. This profile was chosen to illustrate ways in which a real profile can differ from an ideal one in propagation effects. (No attempt has been made to characterize statistical variations over an ensemble of real ocean profiles. The results of this section should not be interpreted as "typical" until such a survey is made.) Cold surface water forms a surface duct that can trap acoustic energy originating within the duct. Ray traces for sources at depths of 300 m and 1000 m illustrate this, as well as the deep-ocean convergence zone. Figure 9 gives contour plots of overpressure from a nonlinear calculation with the 1-kbar

source at a 300-m depth. (No 8-kbar results are contained in Figs. 9 or 10.) Energy trapped in the surface duct is evident for at least 30 km. Past this point, its level falls below the contour level needed to resolve the main wave.

Figure 10 gives peak overdensities versus range for the calculation shown in Figure 9 and for two others with sources (Linear and 1 kbar) at a 1000-m depth in the sound speed profile of Figure 8. This figure shows the sensitivity of environmental focusing to the location of the source relative to the sound channel axis. For ranges greater than 7 km, note the lower overpressures for the 300-m source depth relative to the 1000-m depth (the sound channel axis is at 1250 m). Linear and nonlinear curves for the 1000-m source depth show that in this case nonlinearity has a smaller effect than placement of the source. The nonlinear result for the 1000-m source leads to a particle speed of 2 ft/sec at ranges approaching 30 km. When the same source is placed at the 300-m depth, the over-density and particle speed at a 30-km range are lower by a factor of 2. For this particular sound speed profile, the dominant focus for the 1000-m source depth occurs on a caustic at approximately 2000-m depth. Even though vessels are concerned with only the top few hundred meters of the ocean, this result is not irrelevant. Near islands or bathymetric features, such as a deep, focused wave could be reflected by a sloping bottom and could reach the surface.

Shock propagation results in ideal versus realistic environments for the 1-kbar source at the 1000-m depth (Fig. 5 versus Fig. 10) reveal the following similarities and differences. Nonlinearity in the realistic sound channel reduces the shock strength as a function of range, but by a smaller amount than in the ideal sound channel. Nonlinearity also increases the primary focal range from 24 km to about 27.5 km, or roughly 15% (compared to 10% for the ideal sound channel). The radial width of the focal region is approximately 7 km, as compared to 10 km for the ideal sound channel.

3.0 Summary

NPE model results presented here for a low- to medium-yield device placed near the sound channel axis lead to the following conclusions: (1) impulsive particle speeds of order 2 ft/sec may occur near the first convergence zone or deep-ocean caustic, depending on sound channel details; (2) this may happen in a circular band, which may approach 10 km in width, with average radius typically in the range 30 to 50 km; and (3) the location of the convergence zone may be altered in range and depth by the nonlinearity of the ocean's response to the source. The latter is a model prediction of self-refraction and needs to be verified experimentally. Each NPE calculation to ranges of 60 to 70 km on a grid of 351 by 376 points requires less than 1 CPU hour on a Cray IS. Calculations performed to date represent only a small sample of geometries and environments that may be of concern in defining safe standoff envelopes.

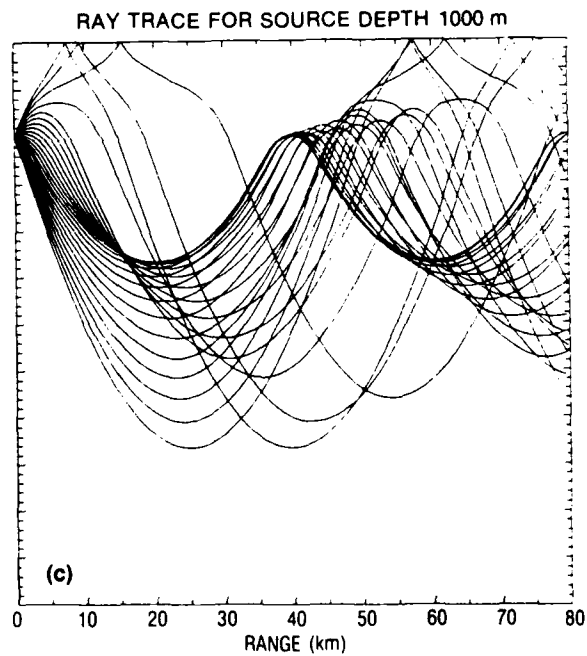
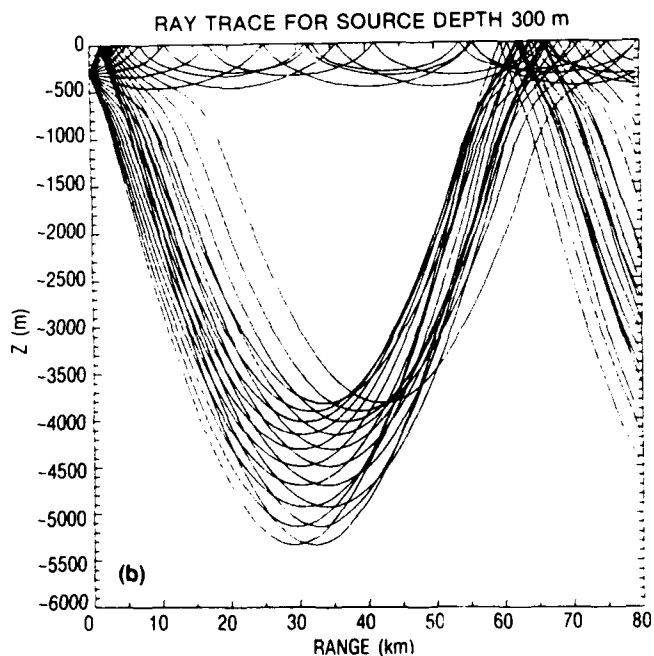
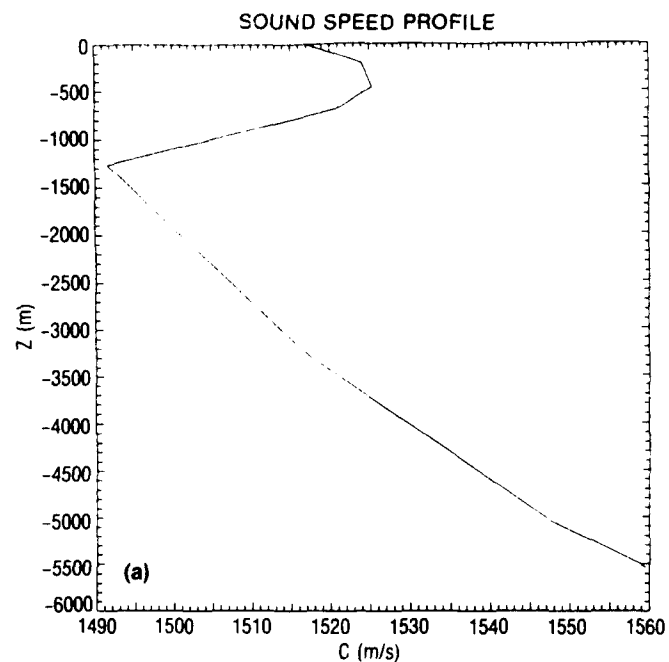


Figure 8. (a) A winter sound speed profile taken near Bermuda. (b) Rays from a source at the 300-m depth illustrate surface ducting. (c) Rays from a source at the 1000-m depth produce deep caustics.

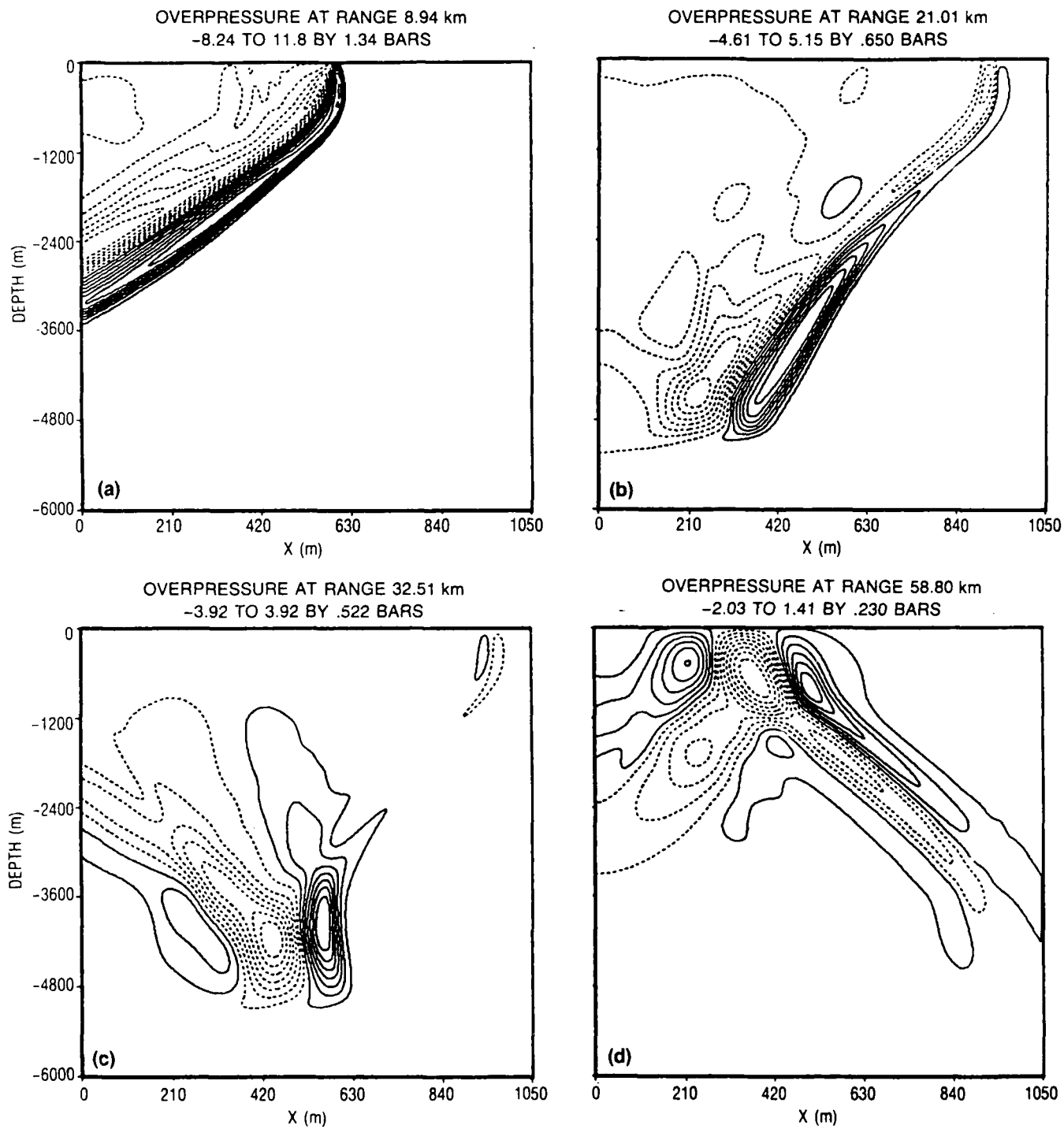


Figure 9. Contour plot snapshots of overpressure through a convergence zone of a 1.13-kbar source at the 300-m depth in the winter sound speed profile of Figure 8. Surface ducting is evident out past 30 km.

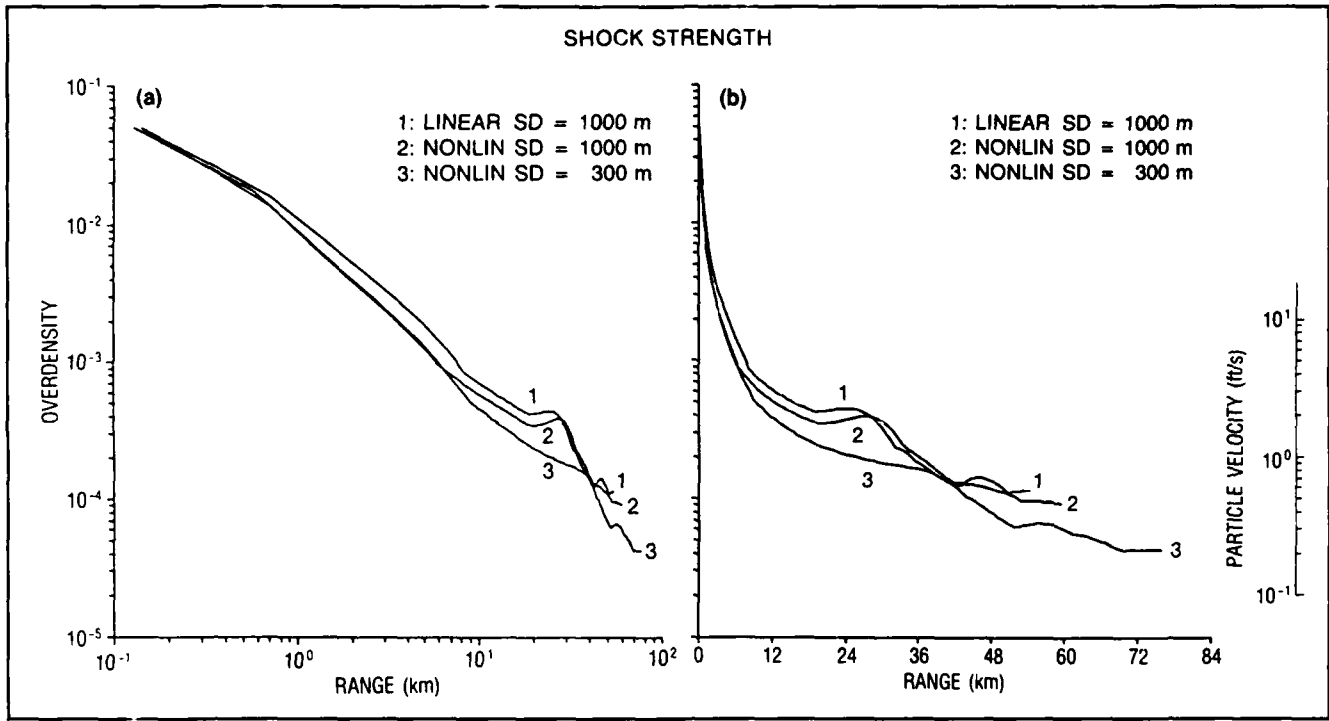


Figure 10. Peak overdensity versus range for a 1.13-kbar source in a winter sound speed profile: (a) log-log; (b) semilog coordinates. Shown are results from a linear calculation for source depth of 1000 m, and nonlinear calculations for source depths of 300 m and 1000 m. Note the lack of focusing (Curve 3) when the source is far from the channel axis. Curve 3 is taken from the calculation of Figure 9.

4.0 References

1. B. E. McDonald and W. A. Kuperman (1987). Time domain formulation for pulse propagation including nonlinear behavior at a caustic. *J. Acoust. Soc. Am.* 81:1406-1417.
2. E. A. Zabolotskaya and R. V. Khokhlov (1969). Quasipplane Waves in the nonlinear acoustics of confined beams. *Sov. Phys. Acoust.* 15:35-40.
3. V. P. Kuznetsov (1971). Equations of nonlinear acoustics. *Sov. Phys. Acoust.* 16:467.
4. B. E. McDonald and W. A. Kuperman (1985). Time domain solution of the Parabolic Equation including nonlinearity. *Comp. & Math. w. Appl.* 11:843-851.

Brooke Farquhar
NORDA Liaison Office
Crystal Plaza #5, Room 802
2211 Jefferson Davis Hwy.
Arlington VA 22202-5000

Director
Defense Mapping Agency Sys Cen
Attn: SGWN
12100 Sunset Hill Rd. #200
Reston VA 22090-3207

NORDA
Code 125 EX
Stennis Space Center MS 39529-5004
(Unlimited only)

Director
Office of Naval Technology
Attn: Dr. P. Selwyn, Code 20
800 N. Quincy St.
Arlington VA 22217-5000

Director
Office of Naval Technology
Attn: Dr. C. V. Votaw, Code 234
800 N. Quincy St.
Arlington VA 22217-5000

Director
Office of Naval Technology
Attn: Dr. M. Briscoe, Code 228
800 N. Quincy St.
Arlington VA 22217-5000

Director
Office of Naval Research
Attn: Dr. E. Hartwig, Code 112
800 N. Quincy St.
Arlington VA 22217-5000

Director
Office of Naval Research
Attn: Code 12
800 N. Quincy St.
Arlington VA 22217-5000

Director
Office of Naval Research
Attn: Dr. E. Silva, Code 10D/10P
800 N. Quincy St.
Arlington VA 22217-5000

Chief of Naval Operations
Navy Department (OP-0962X)
Attn: Mr. R. Feden
Washington DC 20350-2000

Commander
Naval Sea Systems Command
Naval Sea Systems Command Headquarters
Washington DC 20362-5101

Commanding Officer
Naval Civil Engineering Laboratory
Port Hueneme CA 93043

Commander
Naval Air Systems Command
Naval Air Systems Command Headquarters
Washington DC 20361-0001

Pennsylvania State University
Applied Research Laboratory
P.O. Box 30
State College PA 16801

University of Texas at Austin
Applied Research Laboratories
P.O. Box 8029
Austin TX 78713-8029

Johns Hopkins University
Applied Physics Laboratory
Johns Hopkins Rd.
Laurel MD 20707

University of Washington
Applied Physics Laboratory
1013 Northeast 40th St.
Seattle WA 98105

Marine Acoustics, Inc.
2231 Crystal Drive, Suite 410
Arlington VA 22202

Sandia National Laboratory
Attn: Dr. Woodfin, Division 9011
Albuquerque NM 87185-5800

Sandia National Laboratory
Attn: Dr. Farnsworth, Division 1533
Albuquerque NM 87185-5800

Commanding Officer
Defense Nuclear Agency
Attn: SPWE
6801 Telegraph Road
Alexandria VA 22310

REPORT DOCUMENTATION PAGE

Form Approved
OMB No. 0704-0188

Public reporting burden for this collection of information is estimated to average 1 hour per response, including the time for reviewing instructions, searching existing data sources, gathering and maintaining the data needed, and completing and reviewing the collection of information. Send comments regarding this burden estimate or any other aspect of this collection of information, including suggestions for reducing this burden, to Washington Headquarters Services, Directorate for Information Operations and Reports, 1215 Jefferson Davis Highway, Suite 1204, Arlington, VA 22202-4302, and to the Office of Management and Budget, Paperwork Reduction Project (0704-0188), Washington, DC 20503.

| | | | | | |
|---|--|--|--|--|--|
| 1. Agency Use Only (Leave blank). | | 2. Report Date. August 1989 | | 3. Report Type and Dates Covered. | |
| 4. Title and Subtitle. Evidence for Self-Refraction in a Convergence Zone: NPE Model Results | | | | 5. Funding Numbers. <i>Program Element No.</i> 920101 <i>Project No.</i> 0101 <i>Task No.</i> 421 <i>Accession No.</i> DN258097 | |
| 6. Author(s). B. Edward McDonald, *Daniel R. Plante | | | | | |
| 7. Performing Organization Name(s) and Address(es). Ocean Science Directorate Naval Ocean Research and Development Activity Stennis Space Center, Mississippi 39529-5004 | | | | 8. Performing Organization Report Number. NORDA Report 223 | |
| 9. Sponsoring/Monitoring Agency Name(s) and Address(es). Sandia National Laboratory Albuquerque, NM 87185 | | | | 10. Sponsoring/Monitoring Agency Report Number. (N/A) | |
| 11. Supplementary Notes. *Berkeley Research Associates, Springfield, Virginia 22150 | | | | | |
| 12a. Distribution/Availability Statement. Approved for public release; distribution is unlimited. Naval Ocean Research and Development Activity, Stennis Space Center, Mississippi 39529-5004. | | | | 12b. Distribution Code. | |
| 13. Abstract (Maximum 200 words). The nonlinear progressive wave equation (NPE) model was developed by the Naval Ocean Research and Development Activity during 1982-1987 to study nonlinear effects in long-range oceanic propagation of finite amplitude acoustic waves, including weak shocks. The NPE model has been applied to propagation of a generic shock wave (initial condition provided by Sandia Division 1533) in a few illustrative environments. The following consequences of nonlinearity are seen by comparing linear and nonlinear NPE results: (1) a decrease in shock strength versus range (a well-known result of entropy increase at the shock front); (2) an increase in the convergence zone range; and (3) a vertical meandering of the energy path about the corresponding linear ray path. Items (2) and (3) are manifestations of self-refraction. | | | | | |
| 14. Subject Terms. nonlinear propagation, shock focusing, convergence zones | | | | 15. Number of Pages. 11 | |
| | | | | 16. Price Code. | |
| 17. Security Classification of Report. Unclassified | | 18. Security Classification of This Page. Unclassified | | 19. Security Classification of Abstract. Unclassified | |
| | | | | 20. Limitation of Abstract. None | |